Device Level Modeling of Metal-Insulator-Semiconductor Interconnects

Gaofeng Wang, *Senior Member, IEEE*, Xiaoning Qi, *Student Member, IEEE*, Zhiping Yu, *Senior Member, IEEE*, and Robert W. Dutton, *Fellow, IEEE*

***Abstract*—A rigorous model for metal-insulator-semiconductor (MIS) interconnects is presented based on device level simulation results. At the device level, the motion equations of charged carriers and Maxwell's equations are simultaneously solved using a finite element scheme and Newton's method. Simulations provide detailed information regarding field-carrier interactions, semiconductor substrate loss and nonlinearity, as well as slow-wave effect, external bias effect, and screening effect of the charged carriers. An equivalent circuit model of MIS interconnects is established using an energy-based approach. The model consists of an equivalent transmission line that mimics the energy transport characteristics of the actual MIS interconnect, and provides a generalized nonlinear and electronic tunable circuit model suitable for both small-signal and large-signal analysis. Examples are presented to illustrate capabilities and efficiency of the method as well as properties of the equivalent circuit model.**

***Index Terms*—Device level simulation, electromagnetic analysis, electronic controllability, equivalent transmission line model, field-carrier interactions, MIS interconnects, semiconductor nonlinearity, substrate loss.**

I. Introduction

ELECTRICAL performance of on-chip interconnects is increasingly important for high-speed integrated circuits. On-chip wiring delays are now a significant portion of the total chip delay. Interconnect effects such as loss, dispersion, and substrate noise all can degrade circuit performance. Accurate determination of electrical properties for on-chip interconnects represents a crucial design problem. Electrical properties of metal-insulator-semiconductor (MIS) interconnects have been investigated extensively, both experimentally and in theoretical studies [1]–[15]. Theoretical investigations have employed analytical and numerical approaches including circuit models [2], [4], quasi-TEM analysis [5], [6], and full-wave analysis [7]–[15].

Energy dissipations in both semiconductor layers and conductor lines have a significant impact on performance of MIS interconnects. The effect of semiconductor substrate loss was studied using a parallel-plate waveguide model in [2]. It was reported that the resistivity-frequency domain can be divided roughly into three regions: the dielectric quasi-TEM, slow-wave, and skin-effect regions, respectively. Metallic conductor loss has been incorporated in the quasi-TEM analysis in order to construct equivalent circuits [5], [6]. Rigorously speaking, MIS interconnects cannot support TEM waves due to energy dissipation and material inhomogeneities. Detailed analysis of MIS interconnects requires full-wave analysis. Popular approaches for full-wave analysis of MIS interconnects include: mode-matching analysis [7], [8], spectral domain analysis (SDA) [9]–[11], method of lines [12], transmission line matrix method (TLM) [13], finite-difference time-domain method (FDTD) [14], and finite element method (FEM) [15].

When an electromagnetic wave propagates along an MIS interconnect, screening effects of the charged carriers prohibit the electromagnetic field from penetrating deep into the semiconductor, in addition to the attenuation arising from energy dissipation. In order to describe the behavior of the semiconductor as a solid-state plasma, the motion equations of charged carriers should be included directly in the simulation [16], [17]. The nonlinear nature of the semiconductor substrate has been generally ignored in most previous work. The question of when to include the semiconductor nonlinearity, however, has not been answered quantitatively. In order to address the nonlinear characteristics of the carrier motion equations, more comprehensive simulations are required.

To construct equivalent circuit models for the interconnects, a contour integral-based approach has been widely employed [2], [5], [6]. Integrals of the electromagnetic fields over the appropriate contours are used as a convenient definition for voltage and current. These definitions of voltage and current are valid, however, only for TEM waves. When losses are important, the presence of a longitudinal electric field implies that the transverse field components no longer satisfy the static equations. Thus, the definitions for voltage and current in terms of contour integrals of the field components become invalid. In [18], an energy-based approach has been proposed, which abandons the intuitively chosen contour integrals. Rather, it builds an equivalent circuit model based on the power equivalence between the circuit model and the original waveguide.

In this paper, a rigorous model of MIS interconnects is presented based on device level simulations. The motion equations of charged carriers and Maxwell's equations are solved simultaneously, thus preserving the nonlinearity of the semiconductor problem. The energy-based approach is employed to construct the equivalent circuit model from the device level simulation results.

The device level formulation provides details about the field-carrier interactions, substrate loss, and nonlinearity, as well as slow-wave effect, external bias effect, and screening effect of

Manuscript received October 26, 2000; revised March 20, 2001. The review of this paper was arranged by Editor A. H. Marshak.

The authors are with the Center for Integrated Systems, Stanford University, Stanford, CA 94305 USA.

Publisher Item Identifier S 0018-9383(01)05731-8.

the charged carriers. The equivalent circuit model retains information about the semiconductor substrate effects listed above. Moreover, the model provides formulae for the entire frequency-conductivity domain, valid across a wide range of frequencies and substrate doping. Hence, the equivalent circuit model offers a generalized nonlinear and electronic tunable circuit model suitable for both small-signal and large-signal analysis.

II. Device Level Simulation

A typical MIS interconnect structure is shown in Fig. 1(a). For simplicity, the interconnect is modeled as a parallel-plate waveguide structure for the device level simulation [see Fig. 1(b)]. The parallel-plate waveguide structure extends from $y = -\infty$ to $y = \infty$. All physical quantities are assumed to be uniform in the y direction. Moreover, the fundamental mode in a parallel-plate waveguide is a transverse magnetic (TM) mode. For TM modes, the magnetic field has only a y component, whereas the electric field has no y component.

The nonlinear terms of the carrier motion equations can give rise to signal distortion, characterized by high-order harmonics in the frequency domain. For an arbitrary variable $v(\mathbf{r}, t)$

$$v(\mathbf{r}, t) = v_0(x) + \sum_{m=1}^{\infty} v^{(m)}(x) \cdot e^{-m\gamma z} \cdot e^{jm\omega t} \tag{1}$$

where

ω	fundamental frequency;
$\gamma = \alpha + j\beta$	propagation constant;
$v_0(x)$	steady state solution;
$v^{(m)}(x)$	mth harmonic component.

Starting from the motion equations of the charged carriers and Maxwell's equations, one obtains [19], [31]

$$\frac{\partial^2 E_z^{(m)}(x)}{\partial x^2} + m^2(k_c^2 + \gamma^2)E_z^{(m)}(x) = jm\omega\mu\left[J_{nz}^{(m)(r)}(x) + J_{pz}^{(m)(r)}(x)\right] - \frac{qm\gamma}{\varepsilon}\left[p^{(m)}(x) - n^{(m)}(x)\right] \tag{2a}$$

$$jm\omega n^{(m)}(x) = \frac{1}{q}\frac{\partial J_{nx}^{(m)}(x)}{\partial x} - \frac{m\gamma}{q}J_{nz}^{(m)}(x) - u^{(m)}(x) \tag{2b}$$

$$jm\omega p^{(m)}(x) = -\frac{1}{q}\frac{\partial J_{px}^{(m)}(x)}{\partial x} + \frac{m\gamma}{q}J_{pz}^{(m)}(x) - u^{(m)}(x) \tag{2c}$$

and

$$E_x^{(m)}(x) = -\frac{m\gamma}{m^2(k^2+\gamma^2)}\frac{\partial E_z^{(m)}(x)}{\partial x} + \frac{jm\omega\mu}{m^2(k^2+\gamma^2)} \cdot \left[J_{nx}^{(m)}(x) + J_{px}^{(m)}(x)\right] \tag{2d}$$

$$H_y^{(m)}(x) = \frac{1}{jm\omega\mu}\left[\frac{\partial E_z^{(m)}(x)}{\partial x} + m\gamma E_x^{(m)}(x)\right] \tag{2e}$$

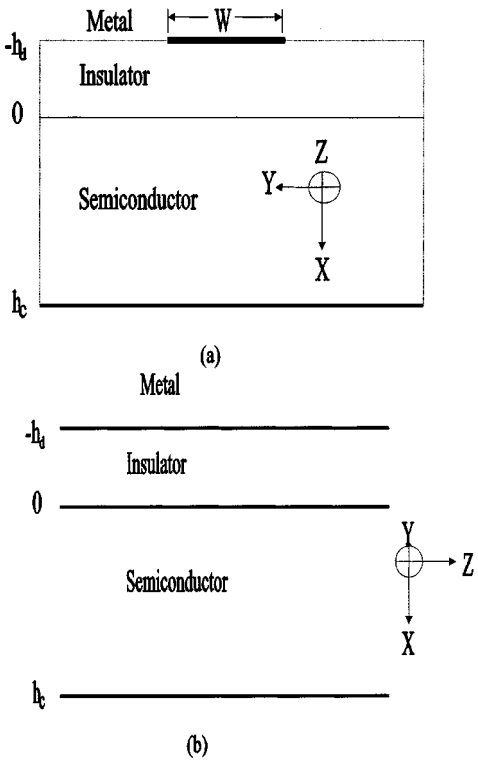

Fig. 1. MIS interconnect structure: (a) configuration and (b) parallel-plate waveguide model.

with

$$(1+jm\omega\tau_n)\mathbf{J}_n^{(m)(0)}(x) = q\mu_n n^{(0)}(x)\mathbf{E}^{(m)}(x) \tag{3a}$$

$$(1+jm\omega\tau_p)\mathbf{J}_p^{(m)(0)}(x) = q\mu_p p^{(0)}(x)\mathbf{E}^{(m)}(x) \tag{3b}$$

$$(1+jm\omega\tau_n)\mathbf{J}_n^{(m)}(x) = q\mu_n\sum_{s=0}^{m}\left[n^{(s)}(x)\mathbf{E}^{(m-s)}(x)\right] + qD_n\nabla n^{(m)}(x) - \hat{\mathbf{z}}qD_n m\gamma n^{(m)}(x) \tag{3c}$$

$$(1+jm\omega\tau_p)\mathbf{J}_p^{(m)}(x) = q\mu_p\sum_{s=0}^{m}\left[p^{(s)}(x)\mathbf{E}^{(m-s)}(x)\right] - qD_p\nabla p^{(m)}(x) + \hat{\mathbf{z}}qD_p m\gamma p^{(m)}(x) \tag{3d}$$

$$\mathbf{J}_n^{(m)(r)}(x) = \mathbf{J}_n^{(m)}(x) - \mathbf{J}_n^{(m)(0)}(x), \quad \mathbf{J}_p^{(m)(r)}(x) = \mathbf{J}_p^{(m)}(x) - \mathbf{J}_p^{(m)(0)}(x) \tag{3e}$$

$$k_c^2 = k^2 - \frac{j\omega\mu\sigma^{(0)}(x)}{m}, \quad \sigma^{(0)}(x) = q\left[\frac{\mu_n n^{(0)}(x)}{1+jm\omega\tau_n} + \frac{\mu_p p^{(0)}(x)}{1+jm\omega\tau_p}\right] \tag{3f}$$

where the meanings of symbols in the above equations are summarized in the following list.

$\mathbf{E}$	Electric field.
$\mathbf{H}$	Magnetic field.
n	Electron density.
p	Hole density.

ϵ Permittivity of the medium
μ Permeability of the medium.
μ_n Effective carrier mobility of electrons.
μ_p Effective carrier mobility of holes
D_n Diffusion coefficients of electrons.
D_p Diffusion coefficients of holes.
τ_n Average collision times of electrons.
τ_p Average collision times of holes
$\mathbf{J}_n$ Electron current density.
$\mathbf{J}_p$ Hole current density.
u Total net recombination rate of electrons and holes.

By accounting for the boundary condition $E_z^{(m)}(-h_d) = 0$ at the metal surface, the field components in the dielectric layer can be obtained as follows:

$$E_z^{(m)}(x) = -\frac{A^{(m)}k_d}{\gamma}\sin[mk_d(x+h_d)] \tag{4a}$$

$$E_x^{(m)}(x) = A^{(m)}\cos[mk_d(x+h_d)] \tag{4b}$$

$$H_y^{(m)}(x) = \frac{j\omega\varepsilon_d A^{(m)}}{\gamma}\cos[mk_d(x+h_d)] \tag{4c}$$

where ε_d and μ_d are the permittivity and permeability of the dielectric layer, and $k_d = \sqrt{\omega^2\mu_d\varepsilon_d + \gamma^2}$. Note that $A^{(1)}$ is an arbitrary constant, depending on the excitation magnitude, while the $A^{(m)}(m > 1)$ are coefficients to be determined.

Boundary conditions at the interface between the insulator and semiconductor, including the ground plane, are as follows:

$$E_z^{(m)}(0^+) = E_z^{(m)}(0^-) = -\frac{A^{(m)}k_d}{\gamma}\sin(mk_d h_d) \tag{5a}$$

$$H_y^{(m)}(0^+) = H_y^{(m)}(0^-) = \frac{j\omega\varepsilon_d A^{(m)}}{\gamma}\cos(mk_d h_d) \tag{5b}$$

$$J_{nx}^{(m)}(0) = J_{px}^{(m)}(0) = 0 \tag{5c}$$

$$E_z^{(m)}(h_c) = 0 \tag{5d}$$

$$n^{(m)}(h_c) = p^{(m)}(h_c) = 0. \tag{5e}$$

For the fundamental mode, eliminating the arbitrary constant $A^{(1)}$ in (5a) and (5b) leads to

$$\frac{E_z^{(1)}(0^+)}{H_y^{(1)}(0^+)} = -\frac{k_d}{j\omega\varepsilon_d}\tan(k_d h_d). \tag{6}$$

Equation (6) provides a nonlinear algebraic equation for determining the propagation constant γ. Given an excitation magnitude $A^{(1)}$, (2a)–(2e) and (6), along with boundary conditions given by (5a), (5c), (5d), and (5e), completely determine the field components, carrier concentrations, and propagation constant for the fundamental mode. Note that the boundary condition (5b) is automatically fulfilled, provided that (5a) and (6) are satisfied.

For higher order harmonics with $m > 1$, (5b) and (2e) are compatible only if one of the following conditions holds:

$$\frac{E_z^{(m)}(0^+)}{H_y^{(m)}(0^+)} = -\frac{mk_d}{jm\omega\varepsilon_d}\tan(mk_d h_d) \tag{7}$$

or

$$A^{(m)} = 0. \tag{8}$$

In general, the propagation constant γ, determined from (6), rarely meets the condition given by (7). Therefore, condition (8) must be imposed as the condition for compatibility. This implies that higher order harmonics due to the semiconductor nonlinearity are confined within the semiconductor and do not penetrate into the insulator.

The solution would not be unique [19], [31] if condition (7) happens to be satisfied—a phenomenal characteristic of shock waves or at resonance. Under the compatibility condition (8), (2a)–(2e) along with the boundary conditions (5a), (5c), (5d), and (5e) completely determine the mth harmonic field components and carrier concentrations (where $m > 1$).

The formulae listed above can be discretized using a standard finite element procedure [20], and then solved using multi-dimensional Newton's method [21] and sparse matrix schemes [22]. Detailed discussion of the numerical solution of the coupled carrier motion and Maxwell's equations can be found in [19], [31].

III. Equivalent Circuit Model

For TM waves, the contour integral definitions of voltage and current using the TEM assumptions are no longer applicable. In this section, the energy-based approach [18] is used to construct an equivalent circuit model from the device level simulation results. The equivalent circuit model is constructed based on the power equivalence between the circuit model and the actual MIS waveguide.

A general form of the transmission line model consists of a series impedance Z per unit length and a shunt admittance Y per unit length, as shown in Fig. 2(a). To build an equivalent transmission line model, the following requirements are prescribed [18].

- The propagation constant for the equivalent transmission line should be identical to the propagation constant γ of the original MIS interconnect.
- The complex time-averaged power traveling down the equivalent circuit is equal to the complex time-averaged power traveling down the original MIS interconnect.

By imposing the above requirements, it can be shown that

$$Z = \gamma\frac{2P(z)}{|I(z)|^2} \tag{9a}$$

$$\frac{1}{Y} = \frac{1}{\gamma}\frac{2P(z)}{|I(z)|^2} \tag{9b}$$

where $I(z)$ is the current flowing through the signal line, and $P(z)$ denotes the complex time-averaged power traveling down the original MIS interconnect. The current flowing through the equivalent transmission line can be defined as the physical current flowing through the signal line

$$I(z) = \iint_{(x,y)\in S_i}\mathbf{J}\cdot\hat{\mathbf{z}}\,dx\,dy \tag{10}$$

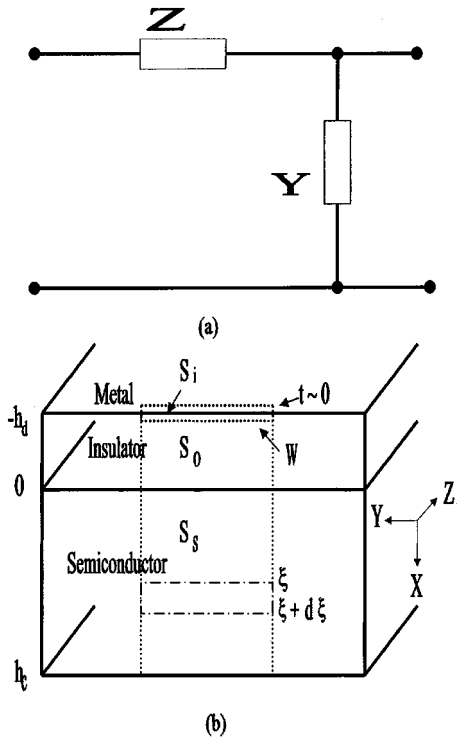

Fig. 2. (a) General form of a transmission line model. (b) Pictorial illustration of S_i, S_0, and S_s in calculation of equivalent circuit elements.

where S_i denotes the cross section of the signal line, as shown in Fig. 2(b). The complex time-averaged power traveling down the original MIS interconnect can be obtained as

$$P(z) = \frac{1}{2T}\int_0^T \left\{ \iint_{(x,y)\in S} [\mathbf{E}\times\mathbf{H}^*]\cdot\hat{\mathbf{z}}\,dx\,dy \right\} dt \quad (11)$$

where $T = 2\pi/\omega$ and $S = S_0 + S_s$ is the cross section of the MIS interconnect, as shown in Fig. 2(b).

Denote

$$E_0(z) = E_x^{(1)}\Big|_{x=-h_d} = A^{(1)}\cdot e^{-\gamma z}. \quad (12)$$

The expression $P(z)$ can be written using two components:

$$P(z) = P_0(z) + P_s(z) \quad (13)$$

with

$$P_0(z) = \frac{1}{2T}\int_0^T \left\{ \iint_{(x,y)\in S_0} [\mathbf{E}\times\mathbf{H}^*]\cdot\hat{\mathbf{z}}\,dx\,dy \right\} dt \quad (14a)$$

$$P_s(z) = \frac{1}{2T}\int_0^T \left\{ \iint_{(x,y)\in S_s} [\mathbf{E}\times\mathbf{H}^*]\cdot\hat{\mathbf{z}}\,dx\,dy \right\} dt \quad (14b)$$

where $P_0(z)$ and $P_s(z)$ capture the insulator (S_0) and semiconductor (S_s) components, respectively.

Note that the surface current on the signal line can be evaluated as $J_{sz}|_{x=-h_d} = (\hat{\mathbf{x}}\times\mathbf{H})|_{x=-h_d}$. Using (4a)–(4c) and (8), expressions (10) and (14a) lead to

$$I(z) = \frac{j\omega\varepsilon_d w}{\gamma} E_0(z) \quad (15)$$

and

$$P_0(z) = \frac{-j\gamma K_d}{2\omega\varepsilon_d w}|I(z)|^2 \quad (16)$$

where the positive real constant K_d is given by

$$K_d = \int_{-h_d}^{0} |\cos[k_d(x+h_d)]|^2\,dx = \frac{1}{2}\left\{ \frac{\sin[2\mathrm{Re}(k_d)h_d]}{2\mathrm{Re}(k_d)} + \frac{\sinh[2\mathrm{Im}(k_d)h_d]}{2\mathrm{Im}(k_d)} \right\}. \quad (17)$$

Note that $K_d \approx h_d$ as $|k_d h_d| \ll 1$. Hence, K_d can be viewed as an equivalent thickness of the insulator layer.

In the semiconductor layer, expanding the field components in terms of series shown in (1) and substituting them into (14b) yields

$$P_s(z) = \sum_{m=1}^{\infty} \frac{P_s^{(m)}}{[A^{(1)}]^{2m}} \left(\frac{|\gamma|}{\omega\varepsilon_d w}\right)^{2m} |I(z)|^{2m} \quad (18)$$

where

$$P_s^{(m)} = \frac{w}{2}\int_0^{h_c} E_x^{(m)}(x)[H_y^{(m)}(x)]^*\,dx. \quad (19)$$

Substituting (13) into (9a) and (9b), one can write

$$Z = (R_0 + j\omega L_0) + (R_s + j\omega L_s) \quad (20a)$$

$$\frac{1}{Y} = \frac{1}{G_0 + j\omega C_0} + \frac{1}{G_s + j\omega C_s} \quad (20b)$$

such that

$$R_0 + j\omega L_0 = \gamma\frac{2P_0(z)}{|I(z)|^2} \quad (21a)$$

$$\frac{1}{G_0 + j\omega C_0} = \frac{1}{\gamma}\frac{2P_0(z)}{|I(z)|^2} \quad (21b)$$

$$R_s + j\omega L_s = \gamma\frac{2P_s(z)}{|I(z)|^2} \quad (21c)$$

$$\frac{1}{G_s + j\omega C_s} = \frac{1}{\gamma}\frac{2P_s(z)}{|I(z)|^2}. \quad (21d)$$

Therefore, one has

$$R_0 + j\omega L_0 = \frac{K_d}{j\omega\varepsilon_d w}(\alpha^2 - \beta^2 + j2\alpha\beta) \quad (22a)$$

$$\frac{1}{G_0 + j\omega C_0} = \frac{K_d}{j\omega\varepsilon_d w} \quad (22b)$$

$$R_s + j\omega L_s = 2\gamma\sum_{m=1}^{\infty} \frac{P_s^{(m)}}{\left[A^{(1)}\right]^{2m}} \left(\frac{|\gamma|}{\omega\varepsilon_d w}\right)^{2m} |I(z)|^{2(m-1)} \quad (22c)$$

$$\frac{1}{G_s + j\omega C_s} = \frac{2}{\gamma}\sum_{m=1}^{\infty} \frac{P_s^{(m)}}{\left[A^{(1)}\right]^{2m}} \left(\frac{|\gamma|}{\omega\varepsilon_d w}\right)^{2m} |I(z)|^{2(m-1)}. \quad (22d)$$

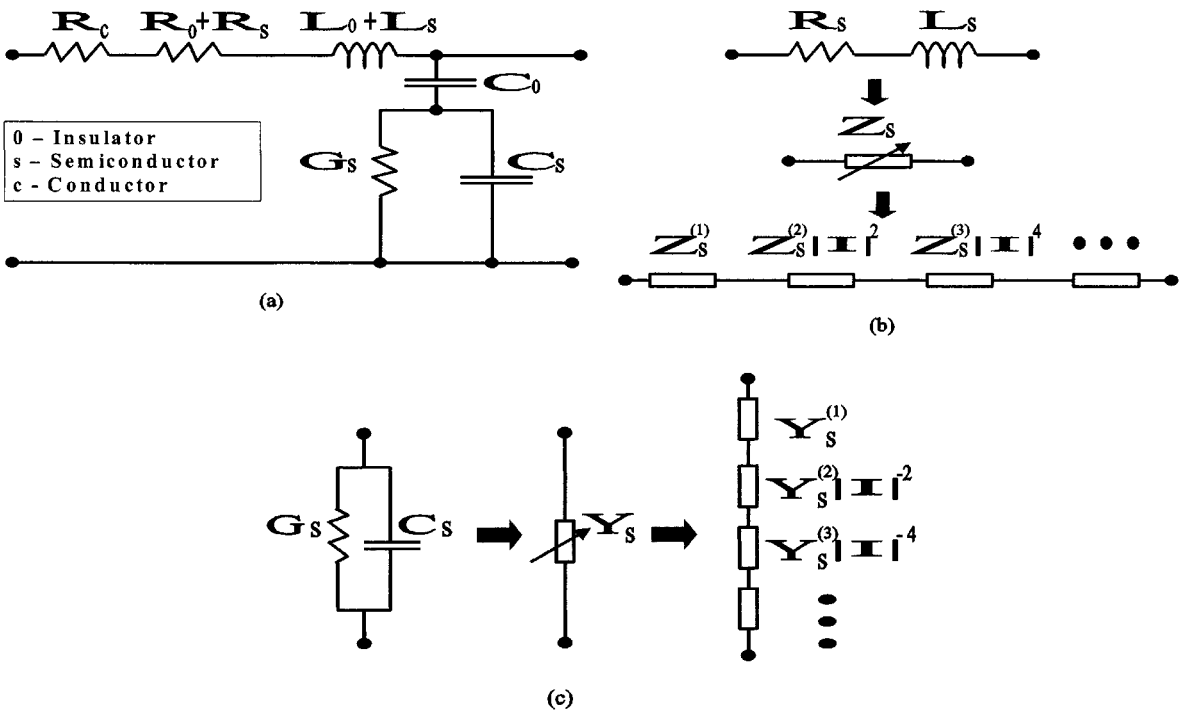

Fig. 3. Equivalent circuit model for MIS interconnects: (a) schematic diagram; (b) impedance Z_s consists of a linear inductance element and many nonlinear impedance elements connected in series; and (c) admittance Y_s consists of a linear admittance element and many nonlinear admittance elements connected in series.

That is

$$R_0 = \frac{2\alpha\beta K_d}{\omega\varepsilon_d w}, \qquad L_0 = \frac{K_d}{\varepsilon_d w}\frac{(\beta^2-\alpha^2)}{\omega^2} \tag{23a}$$

$$C_0 = \frac{\varepsilon_d w}{K_d}, \qquad G_0 = 0 \tag{23b}$$

$$Z_s = R_s + j\omega L_s = Z_s^{(1)} + \sum_{m=2}^{\infty} Z_s^{(m)} |I(z)|^{2(m-1)} \tag{23c}$$

$$\frac{1}{Y_s} = \frac{1}{G_s + j\omega C_s} = \frac{1}{Y_s^{(1)}} + \sum_{m=2}^{\infty} \frac{1}{Y_s^{(m)}} |I(z)|^{2(m-1)} \tag{23d}$$

where

$$Z_s^{(m)} = R_s^{(m)} + j\omega L_s^{(m)} = 2\gamma \left(\frac{|\gamma|}{\omega\varepsilon_d w}\right)^{2m} \frac{P_s^{(m)}}{\left[A^{(1)}\right]^{2m}} \tag{24a}$$

$$Y_s^{(m)} = G_s^{(m)} + j\omega C_s^{(m)} = 1 \Big/ \left[\frac{2}{\gamma}\left(\frac{|\gamma|}{\omega\varepsilon_d w}\right)^{2m} \frac{P_s^{(m)}}{\left[A^{(1)}\right]^{2m}}\right]. \tag{24b}$$

In summary, the equivalent circuit model for the full-wave MIS interconnect model consists of an equivalent transmission line, whose line parameters are given by (23a)–(24b), as shown by Fig. 3(a). The circuit elements R_0, L_0, and C_0 are, respectively, the resistance, inductance, and capacitance per unit length due to the electromagnetic field in the insulator layer, whereas circuit elements R_s, L_s, C_s, and G_s denote, respectively, the resistance, inductance, capacitance, and conductance per unit length due to the electromagnetic field in the semiconductor substrate. Circuit element R_c denotes the resistance per unit length over the signal line, which is not studied here since the signal line has been treated as an ideal conductor.

Note that R_0 is nonzero, even if the insulator medium is lossless. Equation (23a) shows that $R_0 \to 0$ as $\alpha \to 0$. Hence, the existence of nonzero R_0 is due to the influence of the semiconductor loss upon electromagnetic fields in the insulator layer.

Results of the device level simulation [19], [31] show that the mth harmonic field components are proportional to $[A^{(1)}]^m$ in magnitude. The quantity $P_s^{(m)}$ is thus proportional to $[A^{(1)}]^{2m}$ based on using (19). Therefore, the coefficients $R_s^{(m)}$, $L_s^{(m)}$, $G_s^{(m)}$ and $C_s^{(m)}$ given by (24a) and (24b) are independent of the excitation strength. These coefficients are functions of the geometry and material parameters only. Equations (23c) and (23d) state that all the series impedance elements due to the semiconductor effects are connected in series, so do the shunt admittance elements, as shown by Fig. 3(b) and (c).

The first terms in (23c) and (23d) are, respectively, the contributions to the series impedance and shunt admittance from the fundamental mode. The remaining terms are due to higher order harmonics and exhibit nonlinear characteristics as manifested by their dependence on the signal current, given in (23c) and (23d).

For use in the small-signal analysis mode, the nonlinear terms in (23c) and (23d) can generally be neglected. The equivalent circuit model then reduces to a linear transmission line, which has been studied extensively using approaches such as fast Fourier transform (FFT) [23], numerical inversion of the Laplace transform (NILT) [24], asymptotic waveform evaluation (AWE)

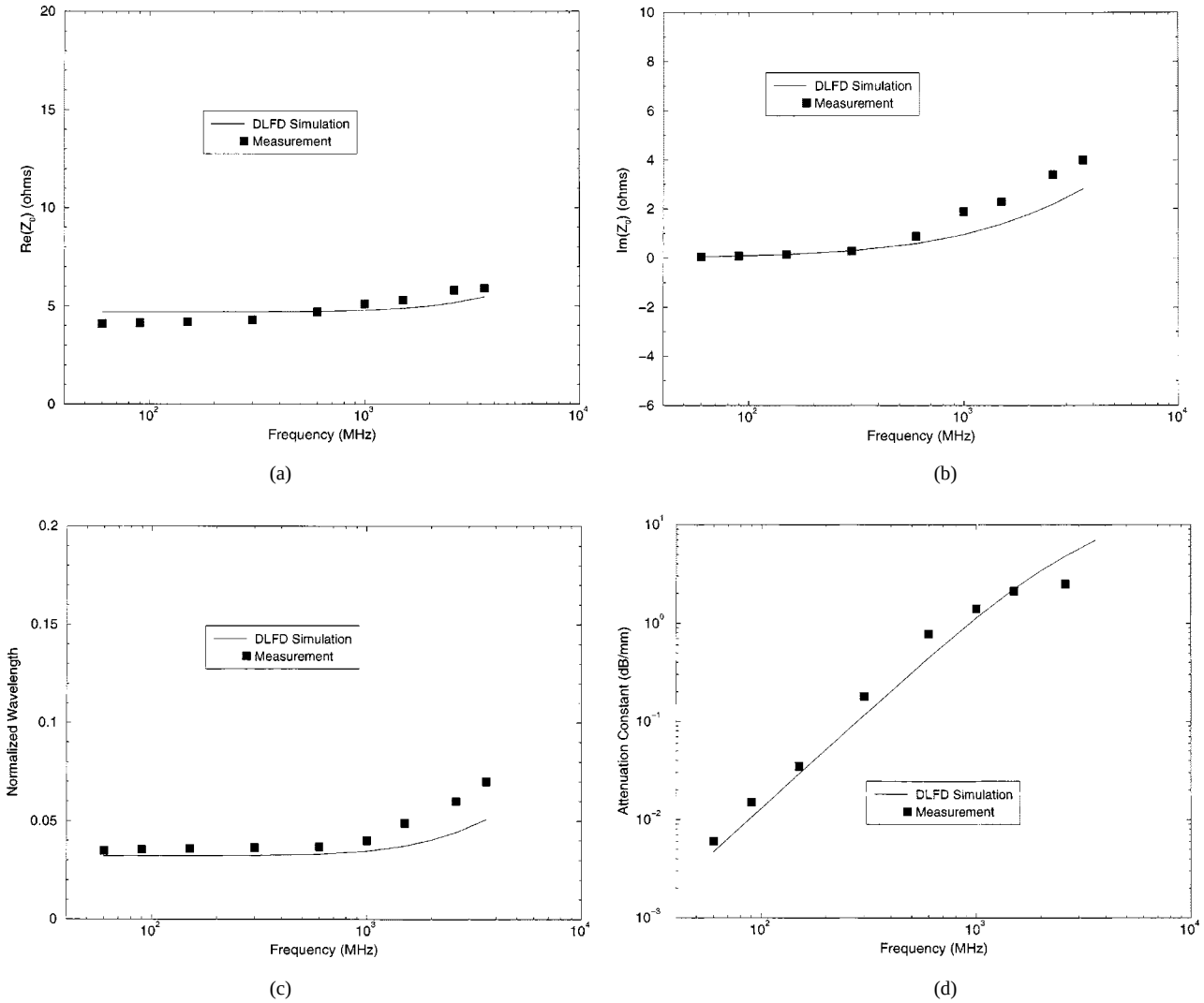

Fig. 4. Comparison between theoretical prediction and measured data: (a) real part of characteristic impedance; (b) imaginary part of characteristic impedance; (c) phase constant; and (d) attenuation constant.

[25], and recursive convolution [26]. Most previous modeling of MIS interconnects has been carried out using only the electromagnetic analysis, with semiconductor effects simply accounted for by virtue of the conductivity, permittivity, and permeability of the semiconductor material. Hence, the basic formula relies on Maxwell's equations and only the linear equivalent circuit elements can be extracted. Since the equivalent circuit model is generally a nonlinear transmission line, this behavior necessitates large-signal analysis. Circuit simulation of nonlinear transmission lines has been addressed by previous research work [27]–[29]. The nonlinear circuit model obtained from this device level scheme can be directly used in nonlinear circuit simulations.

IV. Numerical Results

Consider an MIS interconnect structure consisting of a strip conductor, thin silicon-dioxide layer, and the silicon substrate. The geometrical parameters are as follows: $w = 650\,\mu$m, $h_d = 1\ \mu$m, and $h_c = 250\ \mu$m. The silicon is assumed to be n-type with a donor impurity concentration $N_d = 5 \times 10^{15}\ \text{cm}^{-3}$, which corresponds to a resistivity of $0.9\,\Omega \cdot$ cm. The equivalent circuit model has been created for zero bias conditions using the device level frequency domain (DLFD) scheme described in the preceding sections. The characteristic impedance and propagation constant for this equivalent circuit can be readily obtained using standard transmission line theory. Fig. 4 plots the characteristic impedance and propagation constant versus frequency, in comparison with the measured data from [2]. Generally good agreement is observed in comparing the computed results with the measurements.

Previous analyses of MIS interconnects have employed pure electromagnetic problems where the semiconductor substrate was treated as lossy medium. Hence neither external bias effects nor the inherent semiconductor nonlinearity are considered. In this paper, the semiconductor substrate is described as solid-state plasma, and the external bias effects on characteristics of MIS interconnects are directly included. In addition, the effects due to the semiconductor nonlinearity can be studied.

The external bias effects provide a theoretical foundation for electronic controllable devices. Fig. 5 shows the characteristic impedance and propagation constant versus frequency for three

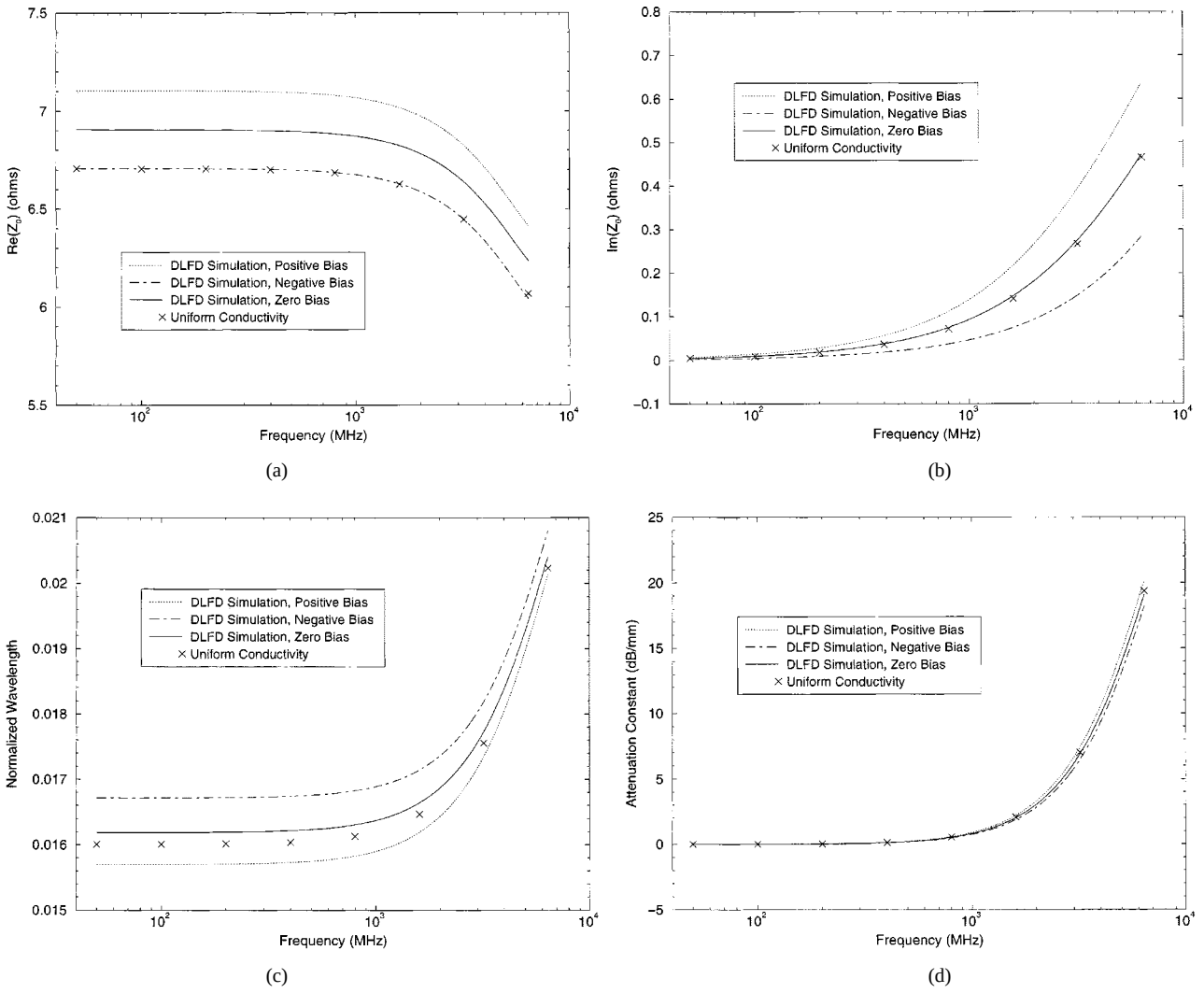

Fig. 5. Characteristic impedance and propagation constant versus frequency and external bias: (a) real part of characteristic impedance; (b) imaginary part of characteristic impedance; (c) phase constant; and (d) attenuation constant.

external bias conditions: $V_0 = -0.2$ V, $V_0 = 0.0$ V, and $V_0 = 0.2$ V. Calculated results using the uniform conductivity model [30] are also shown in Fig. 5. The geometrical parameters used in the calculations are as follows: $w = 90$ μm, $h_d = 0.1$ μm, and $h_c = 100$ μm. The semiconductor substrate is assumed to be n-type silicon, now with donor impurity concentration $N_d = 10^{17}$ cm^{-3}; the insulator is a thin silicon-dioxide layer. It can be observed that the uniform conductivity model generally gives results close to the solutions obtained by this device level scheme for the zero bias. Nevertheless, this scheme is able to provide a quantitative measure to the external bias effects on characteristics of MIS interconnects.

Fig. 6 illustrates the extracted linear and nonlinear equivalent circuit elements for various impurity concentrations. In the calculations, all the parameters are the same as those used for Fig. 4, except for the donor impurity concentration that varies over a range from $N_d = 5\times10^{15}$ cm^{-3} to $N_d = 5\times10^{18}$ cm^{-3}. The operating frequency is assumed to be 1 GHz, and no external bias is applied to this MIS structure. The results obtained using the uniform conductivity model are also shown in the plots for linear circuit elements.

As shown in Fig. 6, the uniform conductivity model gives results close to the numerical solutions from this device level scheme, although apparent differences for $C_s^{(1)}$ and $G_s^{(1)}$ are observed between the two sets of solutions when the semiconductor substrate is heavily doped.

Note that larger $|L_s^{(m)}|$ and $|R_s^{(m)}|$ or smaller $|C_s^{(m)}|$ and $|G_s^{(m)}|$ imply more significant contributions from the mth harmonic $(m > 1)$. Fig. 6 illustrates a case where the nonlinearity becomes less severe when the doping level in the semiconductor substrate increases. More heavily doped semiconductor substrates exhibit greater screening effect, which dramatically reduces the electromagnetic field penetration deep into the semiconductor, thus less wave energy participates in field-carrier interactions.

Fig. 7 depicts the linear and nonlinear equivalent circuit elements versus the insulator thickness. The insulator thickness is varied over a range from $h_d = 0.1$ μm to $h_d = 1$ μm; the operating frequency is assumed to be 6.4 GHz with no external bias applied to the MIS structure. All other parameters are the same as those used for Fig. 5. It is well known that the insulator layer decouples the conductor strip from the semiconductor sub-

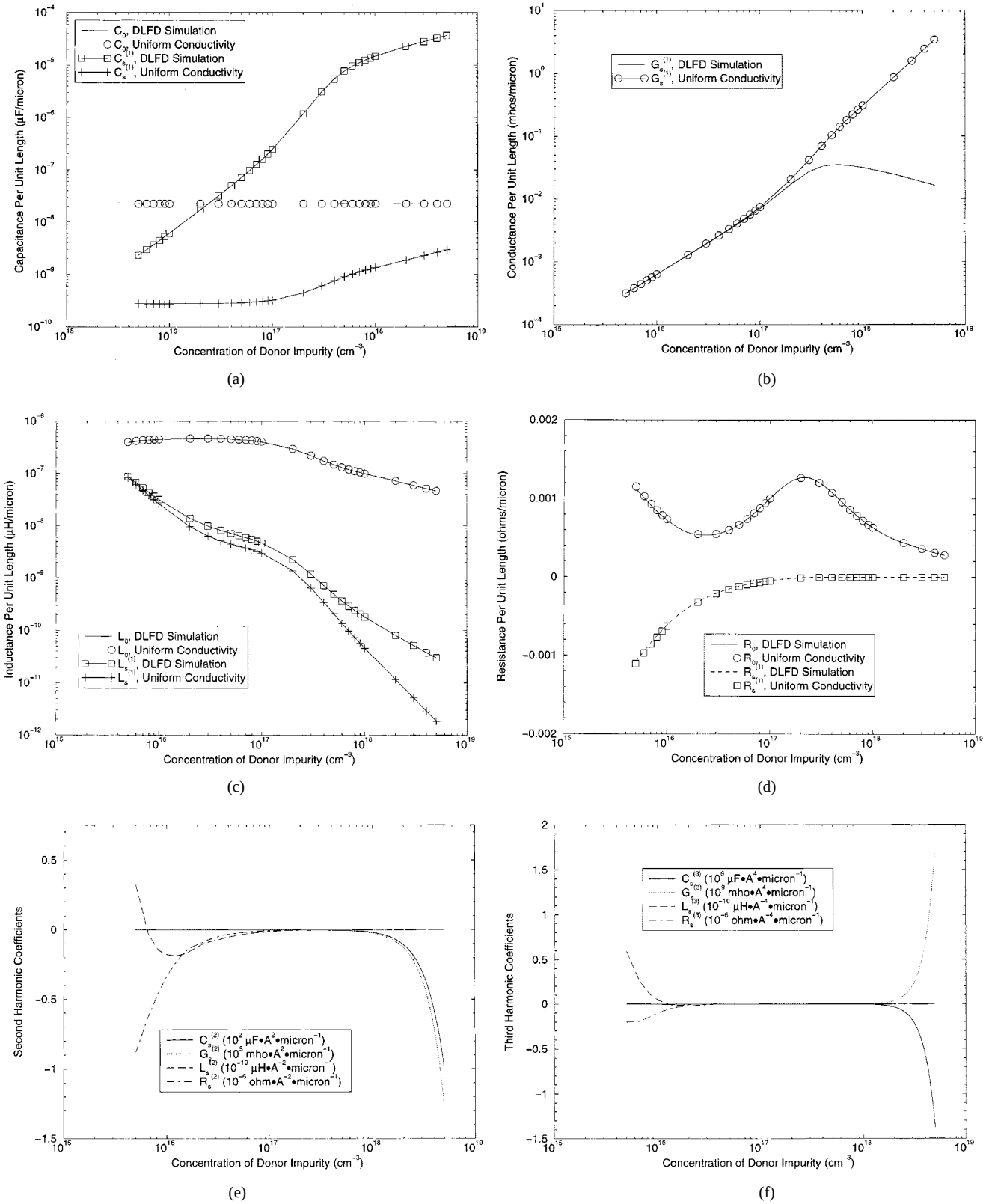

Fig. 6. Equivalent circuit elements versus doping rate: (a) C_0 and $C_s^{(1)}$; (b) $G_s^{(1)}$; (c) L_0, and $L_s^{(1)}$; (d) R_0 and $R_s^{(1)}$; (e) $C_s^{(2)}$, $G_s^{(2)}$, $L_s^{(2)}$, and $R_s^{(2)}$; (f) $C_s^{(3)}$, $G_s^{(3)}$, $L_s^{(3)}$, and $R_s^{(3)}$.

strate and consumes the major portion of the voltage drop. As the insulator thickness increases, it is expected that the electromagnetic field decreases within the semiconductor substrate and thus the MIS structure exhibits less severe nonlinearity. As the insulator layer becomes thicker, smaller $|L_s^{(m)}|$ and $|R_s^{(m)}|$ as well as larger $|C_s^{(m)}|$ and $|G_s^{(m)}|$ are observed for $m = 2$ and $m = 3$ as expected in Fig. 7, which again indicates less nonlinear behavior.

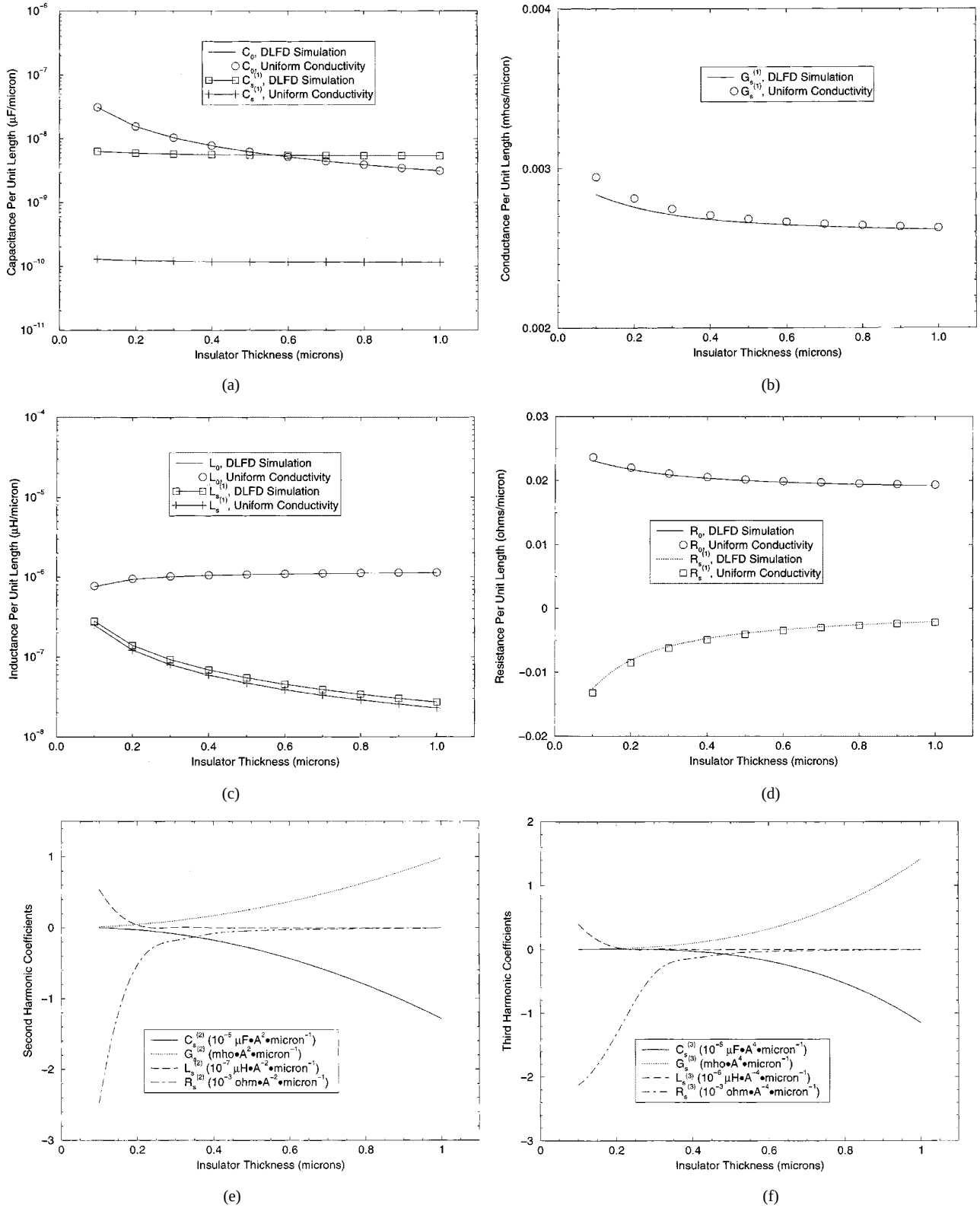

Fig. 7. Equivalent circuit elements versus insulator thickness: (a) C_0 and $C_s^{(1)}$; (b) $G_s^{(1)}$; (c) L_0 and $L_s^{(1)}$; (d) R_0 and $R_s^{(1)}$; (e) $C_s^{(2)}$, $G_s^{(2)}$, $L_s^{(2)}$, and $R_s^{(2)}$; (f) $C_s^{(3)}$, $G_s^{(3)}$, $L_s^{(3)}$, and $R_s^{(3)}$.

V. Conclusion

Device level interconnect simulation provides a rigorous modeling tool for evaluation of MIS interconnects structures. The motion equations for charged carriers and Maxwell's equations are solved simultaneously. Simulation provides a quantitative means to study field-carrier interactions, semiconductor substrate loss and nonlinearity, as well as slow-wave effect, external bias effect, and screening effect of charged carriers. The energy-based approach is used for construction of

the equivalent circuit model based on device level simulation results. The circuit model consists of an equivalent transmission line, which mimics the energy transport characteristics of the actual MIS interconnect. This model provides a generalized nonlinear and electronic tunable circuit model suitable for both small-signal and large-signal analysis.

REFERENCES

[1] T. M. Hyltin, "Microstrip transmission on semiconductor dielectrics," *IEEE Trans. Microwave Theory Tech.*, vol. MTT-13, pp. 777–781, Nov. 1965.

[2] H. Hasegawa, M. Furukawa, and H. Yanai, "Properties of microstrip line on Si–SiO2 system," *IEEE Trans. Microwave Theory Tech.*, vol. MTT-19, pp. 869–881, Nov. 1971.

[3] G. W. Hughes and R. M. White, "Microwave properties of nonlinear MIS and Schottky-barrier microstrip," *IEEE Trans. Electron Devices*, vol. ED-22, pp. 945–956, Oct. 1975.

[4] J. K. Wee, Y. J. Park, H. S. Min, D. H. Cho, M. H. Seung, and H. S. Park, "Modeling the substrate effect in interconnect line characteristics of high-speed VLSI circuits," *IEEE Trans. Microwave Theory Tech.*, vol. 46, pp. 1436–1443, Oct. 1998.

[5] Y. R. Kwon, V. M. Hietala, and K. S. Champlin, "Quasi-TEM analysis of slow-wave mode propagation on coplanar microstructure MIS transmission lines," *IEEE Trans. Microwave Theory Tech.*, vol. MTT-35, pp. 545–551, June 1987.

[6] K. W. Goossen and R. B. Hammond, "Modeling of picosecond pulse propagation in microstrip interconnections on integrated circuits," *IEEE Trans. Microwave Theory Tech.*, vol. 37, pp. 469–478, March 1989.

[7] Y. Fukuoka, Y. Shih, and T. Itoh, "Analysis of slow-wave coplanar waveguide for monolithic integrated circuits," *IEEE Trans. Microwave Theory Tech.*, vol. MTT-31, pp. 567–573, July 1983.

[8] R. Sorrentino, G. Leuzzi, and A. Silbermann, "Characteristics of metal-insulator-semiconductor coplanar waveguide for monolithic microwave circuits," *IEEE Trans. Microwave Theory Tech.*, vol. MTT-32, pp. 410–416, Oct. 1984.

[9] T. G. Livernois and P. B. Katehi, "A generalized method for deriving the space-domain Green's function in a shielded, multilayer substrate structure with applications to MIS transmission lines," *IEEE Trans. Microwave Theory Tech.*, vol. 37, pp. 1761–1767, Nov. 1989.

[10] J. P. K. Gilb and C. A. Balanis, "MIS slow-wave structures over a wide range of parameters," *IEEE Trans. Microwave Theory Tech.*, vol. 40, pp. 2148–2154, Dec. 1992.

[11] J. C. Liou and K. M. Lau, "Analysis of slow-wave transmission lines on multi-layered semiconductor structures including conductor loss," *IEEE Trans. Microwave Theory Tech.*, vol. 41, pp. 814–829, May 1993.

[12] K. Wu and R. Vahldieck, "Hybrid-mode analysis of homogeneously and inhomogeneously doped low-loss slow-wave coplanar transmission lines," *IEEE Trans. Microwave Theory Tech.*, vol. 39, pp. 1348–1360, Aug. 1991.

[13] S. Chen, R. Vahldieck, and J. Huang, "Rigorous analysis of mode propagation and field scattering in silicon-based coplanar MIS slow wave structures with abrupt transitions to transmission lines on normal substrate," *IEEE Trans. Microwave Theory Tech.*, vol. 44, pp. 2487–2494, May 1996.

[14] T. Shibata and E. Sano, "Characterization of MIS structure coplanar transmission lines for investigation of signal propagation in integrated circuits," *IEEE Trans. Microwave Theory Tech.*, vol. 38, pp. 881–890, July 1990.

[15] M. Aubourg, J. Villotte, F. Godon, and Y. Garault, "Finite element analysis of lossy waveguide—Applications to microstrip lines on semiconductor substrate," *IEEE Trans. Microwave Theory Tech.*, vol. MTT-31, pp. 326–330, April 1983.

[16] C. M. Krowne and G. B. Tait, "Propagation in layered biased semiconductor structures based on transport analysis," *IEEE Trans. Microwave Theory Tech.*, vol. 37, pp. 711–722, April 1989.

[17] K. Han and T. T. Y. Wong, "Space-charge wave considerations in MIS waveguide analysis," *IEEE Trans. Microwave Theory Tech.*, vol. 39, pp. 1126–1132, July 1991.

[18] J. R. Brews, "Transmission line models for lossy waveguide interconnections in VLSI," *IEEE Trans. Electron. Devices*, vol. ED-33, pp. 1356–1365, Sept. 1986.

[19] G. Wang, R. W. Dutton, and C. S. Rafferty, "Device level simulation of wave propagation along metal-insulator-semiconductor interconnects," *IEEE Trans. Microwave Theory Tech.*, to be published.

[20] T. J. R. Hughes, *The Finite Element Method: Linear Static and Dynamic Finite Element Analysis*. Englewood Cliffs, NJ: Prentice-Hall, 1987.

[21] J. E. Dennis and R. B. Schnabel, *Numerical Methods for Unconstrained Optimization and Nonlinear Equations*. Englewood Cliffs, NJ: Prentice-Hall, 1983.

[22] G. H. Golub and C. F. Van Loan, *Matrix Computations*, 3rd ed. Baltimore, MD: Johns Hopkins Univ. Press, 1996.

[23] A. R. Djordjevic, T. K. Sarkar, and G. F. Harrington, "Time-domain response of multiconductor transmission lines," *Proc. IEEE*, vol. 75, no. 6, pp. 743–764, June 1987.

[24] R. Griffith, E. Chiprount, Q. J. Zhang, and M. Nakhla, "A CAD framework for simulation and optimization of high-speed VLSI interconnects," *IEEE Trans. Circuits Syst.*, vol. 39, pp. 893–906, Nov. 1992.

[25] J. E. Bracken, V. Raghavan, and R. A. Rohrer, "nterconnect simulation with asymptotic waveform evaluation (AWE)," *IEEE Trans. Circuits Syst.*, vol. 39, pp. 869–878, Nov. 1992.

[26] S. Lin and E. S. Kuh, "Transient simulation of lossy interconnects based on the recursive convolution formulation," *IEEE Trans. Circuits Syst.*, vol. 39, pp. 879–892, Nov. 1992.

[27] F. Fallside and D. T. Bickley, "Nonlinear delay line with constant characteristic impedance," in *Proc. Inst. Elec. Eng.*, vol. 113, Feb. 1966, pp. 263–270.

[28] S. K. Mullick, "Propagation of signals in nonlinear transmission lines," *IBM J. Res. Develop.*, vol. 11, pp. 558–562, Sept. 1967.

[29] M. M. Turner, G. Branch, and P. W. Smith, "Methods of theoretical analysis and computer modeling of the shaping of electrical pulses by nonlinear transmission lines and lumped-element delay lines," *IEEE Trans. Electron Devices*, vol. 38, pp. 810–816, April 1991.

[30] D. F. Williams, "Metal-insulator-semiconductor transmission lines," *IEEE Trans. Microwave Theory Tech.*, vol. 47, pp. 176–181, Feb. 1999.

[31] G. Wang, "Coupled electromagnetic and device level investigations of metal-insulator-semiconductor interconnects," Ph.D. dissertation, Stanford Univ., Stanford, CA, Feb. 2001.

Gaofeng Wang (S'93–M'95–SM'01) was born in Hubei, China, on December 24, 1965. He received the Ph.D. degree in electrical engineering from the University of Wisconsin, Milwaukee, and the Ph.D. degree in scientific computing from Stanford University, Stanford, CA, in 1993 and 2001, respectively.

From 1988 to 1990, he was with the Department of Space Physics, Wuhan University, China, where he was involved in research and teaching of radiowave propagation in ionosphere and numerical methods for electromagnetic waves and fields. From 1990 to 1993, he was a Research Assistant at the Department of Electrical Engineering of the University of Wisconsin. From 1993 to 1996, he was a Scientist at the Tanner Research, Inc., Pasadena, CA. From 1996 to 2001, he was a Principal Engineer at the Synopsys, Inc., Mountain View, CA. Since 2000, he has been a Chief Scientist at Intpax, Inc., Cupertino, CA. In summer 1999, he served as a Consultant at the Bell Laboratories, Lucent Technologies, Murray Hill, NJ. Since 1998, he has been a member of Dutton's Technology CAD group at Stanford University. His research and development interests include electromagnetic theory, microwave engineering, computational electromagnetics, electronic design automation (EDA) software, signal integrity analysis, device modeling, wavelet applications in numerical analysis and image processing, and optical engineering. He has published over 50 technical papers, including 25 articles in leading archival scientific journals.

Xiaoning Qi (S'00) received the B.S. and M.S. degrees in electrical engineering from Hangzhou Institute of Electronics Engineering, Hangzhou, China, in 1988 and 1991, respectively. He is currently pursuing the Ph.D. degree in the Department of Electrical Engineering, Stanford University, Stanford, CA.

His research interests are VLSI interconnect modeling, RF circuit interconnect and package modeling, VLSI performance driven physical design including timing driven floorplanning, placement, and routing. He held a summer position at Synopsys, Inc., Mountain View, CA, in 1999. His research activities at Stanford University include on-chip inductance modeling of VLSI interconnects including power/ground lines; three-dimensional (3-D) geometry modeling and parasitics extraction of IC packaging for RF devices; layout-based 3-D solid-modeling of IC structures and interconnects including electrical parameter extraction, etc. He has published 23 technical papers.

Zhiping Yu (M'90–SM'90) received the B.S. degree from Tsinghua University, Beijing, China, in 1967, and the M.S. and Ph.D. degrees from Stanford University, Stanford, CA, in 1980 and 1985, respectively.

He is presently a Senior Research Scientist, Department of Electrical Engineering, Stanford University, and also holds a Full Professorship at Tsinghua University. His research interests focus on IC process, device, and circuit simulation, and in particular, the numerical techniques and modeling of RF and heterostructure devices. He has been involved in efforts to develop a simulation package for optoelectronic devices and 3-D solid modeling for ICs. Besides the full-time university research, he is a Consultant to HP ULSI Lab, HP, developing advanced transport models for sub-quarter-micron CMOS technology, including quantum mechanical effects.

Dr. Yu is currently serving as the Associate Editor of IEEE TRANSACTIONS ON COMPUTER-AIDED DESIGN OF INTEGRATED DESIGN CIRCUITS AND SYSTEMS, responsible for TCAD-related fields.

Robert W. Dutton (S'67–M'70–SM'80–F'84) received the B.S., M.S., and Ph.D. degrees from the University of California, Berkeley, in 1966, 1967, and 1970, respectively.

He has held summer staff positions at Fairchild, Bell Telephone Laboratories, Hewlett-Packard, IBM Research, and Matsushita during 1967, 1973, 1975, 1977, and 1988, respectively. He is currently Professor of Electrical Engineering at Stanford University, Stanford, CA, and Director of Research in the Center for Integrated Systems. His research interests focus on integrated circuit process, device, and circuit technologies—especially the use of computer-aided design (CAD) in device scaling and for RF applications. He has published more than 200 journal articles and graduated more than four dozen doctorate students.

Dr. Dutton was the winner of the 1987 IEEE J. J. Ebers and 1996 Jack Morton Awards, received 1988 Guggenheim Fellowship to study in Japan, and was elected to the National Academy of Engineering in 1991. He was also honored with the Jack A. Morton Award in 1996 and the C&C Prize (Japan) in 2000. He was Editor of the IEEE TRANSACTIONS ON COMPUTER-AIDED DESIGN OF INTEGRATED CIRCUITS AND SYSTEMS from 1984 to 1986.